RSC Advances

PAPER

View Article Online
View Journal | View Issue



Cite this: *RSC Adv.*, 2025, **15**, 46009

# Investigating the *in vitro* antibiofilm, antioxidant and photocatalytic potential of iron oxide nanoparticles biofabricated from *Bauhinia variegata*

Rasti Abbas, Saima Muzammil, Mohsin Khurshid and Sumreen Hayat*

The emergence of multidrug-resistant (MDR) bacteria poses a critical challenge to modern medicine, necessitating the development of novel and effective therapeutic strategies. The present study introduces a green synthesis approach for producing iron oxide (FeO) nanoparticles using aqueous leaf extract of *Bauhinia variegata* L., as both reducing and stabilizing agents. Characterization confirmed the formation of highly crystalline spherical FeO nanoparticles, typically under 100 nm in diameter. The plant-derived secondary metabolites such as phenolics, tannins, and flavonoids identified *via* FTIR spectroscopy were confirmed to be associated with the nanoparticles, contributing to their promising biological activities. FeO nanoparticles demonstrated broad-spectrum antibacterial efficacy against a panel of clinically relevant MDR pathogens (*A. baumannii*, *E. coli*, *K. pneumoniae*, *P. aeruginosa*, *E. faecium*, and *S. aureus*), and their antibacterial potential might be attributed to the activation of reactive oxygen species (ROS) *via* the Fenton reaction. Furthermore, the nanoparticles exhibited significant anti-biofilm activity, inhibiting initial bacterial attachment and slime production, and achieved high levels of biofilm inhibition (69.77–79%) across all tested bacterial strains. In addition to their antibacterial potential, FeO nanoparticles showed strong antioxidant activity against DPPH, ABTS, and $H_2O_2$ radicals. They also displayed excellent photocatalytic degradation of Congo red dye (89% degradation), showcasing high degradation efficiency that is directly linked to their small size and high crystallinity. Findings of this study underscore the significant potential of FeO nanoparticles for biomedical and environmental applications because of their promising antibacterial, antibiofilm, antioxidant and photocatalytic actions and a greener route for the synthesis of these nanoparticles.

Received 29th September 2025
Accepted 3rd November 2025

DOI: 10.1039/d5ra07391j

rsc.li/rsc-advances



## 1. Introduction

The emergence and rapid dissemination of antibiotic-resistant bacteria have become one of the greatest threats faced by human and animal health, food security and safety, and agricultural and economic development around the globe.[1] This issue is compounded by the ability of these organisms to form biofilms, which protect them from various antibacterial agents as well as from the host's immune system, thereby endowing them with the potential to cause recurrent and persistent infections.[2,3] Antibiotic resistance is one of the biggest public health challenges of our time as a result of which in the U.S., annually at least 2.8 million people get an antibiotic-resistant infection, and more than 35 000 people die.[4] Consequently, there is an imperative need for effective alternatives to combat infections caused by these resistant, biofilm-forming pathogens. Nanotechnology offers promising solutions, providing the foundation for developing efficient nanomaterials capable of overcoming resistance and enhancing drug delivery systems, positioning them as effective antimicrobial treatments.[5–7]

The progress of nano-technology has steered to advancement of distinct nano-molecules with photocatalytic features, retaining shifting properties that play a crucial role in different fields of study especially for the decontamination of environment. Therefore, an upsurge in this chase intended for effective nanoparticles due to various uses, resulting in an increased focus on their production.[8] These nanoparticles have outstanding properties such as stability, sensitivity, increased surface area and reactivity, making them a more useful tool to replace indecisive therapies.[9] Different metal oxides such as magnesium oxide (MgO), silver oxide (AgO), copper oxide (CuO), titanium oxide (TiO), zinc oxide (ZnO), zirconium oxide (ZrO) and iron oxide (FeO) have been focused for their diverse applications as nanoparticles.[10–15]

Amongst them, FeO nanoparticles have earned importance as a major biomedical tool due to their non-toxic nature and exceptional properties besides the added benefits such as

*Institute of Microbiology, Government College University, Faisalabad, Pakistan. E-mail: sumreenhayat@gcuf.edu.pk*

reduced cost, elevated electrochemical activity and the extended lead time. These nanoparticles have also been reported to cross the blood–brain barrier due to their smaller size, and hence, considered as an effective medicinal option.[16,17] FeO nanoparticles showed encouraging antimicrobial activity and also helped in the removal of antibiotics from waterways.[18,19] Thus, understanding the variable characteristics of these nanoparticles in different fields, for instance, catalysis, antioxidants, antidiabetic activities, environment and several other biomedical applications has gained interest.[20,21] FeO nanoparticles can increasingly be utilized for numerous environmental applications due to their efficiency and strong catalytic potential. These nanoparticles can efficiently adsorb heavy metals, degrade organic pollutants *via* Fenton-like reactions, and enable magnetic separation for reusable water purification systems. The eco-friendly synthesis method enhances scalability and minimizes harmful byproducts, making it a promising alternative to conventional chemical processes.[22]

Various methods are used for the synthesis of nanomaterials such as physical, chemical and biological (green) routes.[23] These physical and chemical methods often involve different chemicals such as carbon monoxide, dimethylformamide, hydrogen peroxide, sodium borohydride, hydroxylamine hydrochloride and hydrazine as reducing agents, which can be toxic to the environment. The increasing awareness over environmental sustainability and the urgent need for eco-friendly approaches for nanomaterial synthesis have driven the scientific community to explore a green route of synthesis.[24]

Biological/green methods employ natural compounds present in either plants or microorganisms as capping and reducing agents. The green route for the synthesis of nanomaterials offers various advantages such as biocompatibility, cost-effectiveness, simplicity, biodegradability, large-scale production and eco-friendliness.[25,26] Plants have been increasingly recognized as valuable biological sources for the green synthesis of nanoparticles due to their exceptional stability, accessibility and scalability, which does not require special storage facilities. During the synthesis process, plant extracts play a crucial role of stabilizing and reducing agents since they contain a variety of secondary metabolites such as polyphenols, flavonoids, sugars and terpenoids, facilitating the reduction of metal ions and synthesis of metallic oxide nanoparticles.[27]

The presence of diverse biomolecules in different plant sources can result in the synthesis of nanoparticles with varying antibacterial and antibiofilm potential. Thus, it is imperative to hunt for various biological sources for the green synthesis of nanoparticles. *B. variegata* is a flowering plant belonging to 'Leguminosae' family, subfamily 'Caesalpiniaceae'. It is a native plant of Southeast Asia, Western India and China. The genus *Bauhinia* has more than 200 species. It is well known as orchid tree (mountain ebony), and in Pakistan, it is locally known as kachnar. It is a medium-sized deciduous plant, cultivated due to the sophisticated looks of its flowers.[28] Several studies have reported the antimicrobial, antioxidant and anti-diabetic activities of leaf extracts of *B. variegata* due to the presence of flavonoids and polyphenols. A variety of bioactive compounds such as flavonoids, tannins, terpenoids, alkaloids and polyphenols are present in *Bauhinia variegata* that might contribute to the green synthesis of nanoparticles by acting as reducing and stabilizing agents.[29,30] The plant-based capping agents on the surface of nanoparticles improve biocompatibility, reducing nonspecific toxicity. This coating prevents nanoparticles from aggregating into larger, less active clumps. The stability conferred by this coating helps maintain small size, which is critical for their enhanced activity, making them suitable for medical uses. The *Bauhinia variegata* extract increases the effect of FeO nanoparticles through a synergistic process involving the phytochemicals. These phytochemicals convert iron ions from ferric chloride into FeO nanoparticles. For instance, phenolic compounds have hydroxyl groups that donate electrons, ions reducing the metal to their neutral state to form the nanoparticle core.[31,32]

Green synthesis of FeO nanoparticles was performed using plant sources as reducing and stabilizing agents in different studies.[33] However, the novelty of this study resides in a simple, cost-effective and green approach to synthesize FeO nanoparticles from *B. variegata.* This study was conducted to biosynthesize FeO nanoparticles from *B. variegata* leaf extract and to check biological applications including antibacterial, antibiofilm, antioxidant and photocatalytic potential. This environmentally friendly approach seeks to minimize the reliance on toxic chemicals and to lessen the overall hazardous impacts on the environment associated with fabrication processes. Characterization of these nanoparticles was done using standard techniques such as UV-vis spectroscopy, XDR, FTIR spectroscopy and SEM and further assessed for antioxidant, antibacterial and antibiofilm effects. Additionally, the research investigated the dye degradation capability of these green synthesized nanoparticles. The utilization of FeO nanoparticles for the degradation of Congo red dye offers an effective remediation strategy while exploring their antioxidant and antibiofilm potential will shed light on their possible biomedical implications.

## 2. Materials and methods

### 2.1 Materials

All the chemicals used in this study were purchased from Sigma-Aldrich (St. Louis, MO, USA), unless otherwise stated. Fresh leaves of the plant (*Bauhinia variegata* L.) were locally collected (Botanical Garden of Government College University) during early spring and botanical identification was authenticated by Prof. Dr Naeem Iqbal, from the Department of Botany, Government College University, Faisalabad (Voucher no. GCU-365).

### 2.2 Bacterial strains

MDR bacterial strains were collected from the Institute of Microbiology, Government College University, Faisalabad (GCUF), Pakistan. Gram-positive bacteria such as *E. faecium* (Accession No. KX609796.1) and *S. aureus* (Accession No. KX685332.1) and Gram-negative bacteria such as *A. baumannii* (Accession No. MH605335), *K. pneumoniae* (Accession No.

MF953599), *E. coli* (Accession No. KY305421.1) and *P. aeruginosa* (Accession No. MK793697.1) were included in the present study. These organisms were aerobically cultured at 37 °C for 24 hours, and their cell density was adjusted to 0.5 McFarland ($1 \times 10^8$ CFU $ml^{-1}$) prior to all tests.[34,35]

**2.2.1 Green synthesis of FeO nanoparticles.** The fresh leaves of *Bauhinia variegata* L. were cleaned thrice using deionized water, for eliminating dust particles and impurities. These cleaned leaves were kept under shade for a week and dried, and then, 25 grams of fine sliced leaves were placed in a 200 ml flask and 100 ml of deionized water was poured into the flask. This mixture was further warmed at 80 °C for 30 minutes and then cooled down. The cooled aqueous leaf extract was passed through a filter (Whatman filter paper No.1). The plant leaf extract gained after filtration was utilized for FeO nanoparticle synthesis.

Green synthesis of FeO nanoparticles was achieved in accordance with the protocol described earlier.[33] The aqueous leaf extract of *Bauhinia variegata* L. was combined with 0.01 M $FeCl_3 \cdot 6H_2O$ solution to synthesize FeO nanoparticles. Further, the extract was prepared by drenching leaves in autoclaved water for about 24 hours. The formulated $FeCl_3$ solution was added dropwise into plant leaf extract with constant stirring. The synthesis of FeO nanoparticles was examined by change in colour from a brownish red solution to a black precipitate. The solution was centrifuged at 4000 rpm for about 15 minutes, and the pellet was washed with deionized water. The subsequent pellet was dried in a hot air oven at about 90 °C (for 2 hours) to achieve black, purified nanoparticles. Moreover, the mechanism of green synthesis of FeO nanoparticles from the leaf extract of *B. variegata* is also shown in Fig. 1. The stock solution (1 mg $ml^{-1}$) of these nanoparticles was prepared by dissolving nanoparticles in dimethyl sulfoxide (DMSO 2.0%), and this suspension was sonicated at 30 °C for half an hour.

**2.2.2 Characterization of FeO nanoparticles.** FeO nanoparticles were characterized by different techniques, *i.e.*, UV-visible spectroscopy, FTIR (Fourier transformed infra-red) spectroscopy, XRD (X-ray diffraction) and SEM (scanning electron microscopy). To study the optical properties of the product and to confirm the formation of NPs, UV-vis spectroscopy was performed in the range of 200–800 nm using a spectrophotometer (HITACHI UH5300). For the functional groups analysis including composition and occurrence of different groups present in biofabricated FeO nanoparticles, Fourier transform infra-red (FTIR) spectroscopy was performed using a Bruker spectrometer (Germany) in the range of 600–4000 $cm^{-1}$ to obtain absorption ranges, revealing the presence of different functional groups.[27,36] For elemental and structural analyses, X-ray diffraction (XRD) was performed using a current of 40 mA, a source of cu-K$\alpha$ radiation with 45 kV voltage at $2\theta$ in the range from 10° to 80°. For observing the morphology, SEM was performed employing carbon tape coated with thin films of FeO nanoparticles dried for 5 minutes. The images were acquired using a magnification of 30 000× and operated at 20 kV voltage using a scanning microscope.[37]

### 2.3 *In vitro* antibacterial activity of FeO nanoparticles

**2.3.1 Agar well diffusion method.** The antibacterial potential of FeO nanoparticles was checked against MDR bacteria by an agar well diffusion method.[33] First, 100 µl of standardized bacterial inoculum was spread on Muller Hinton (MH) agar

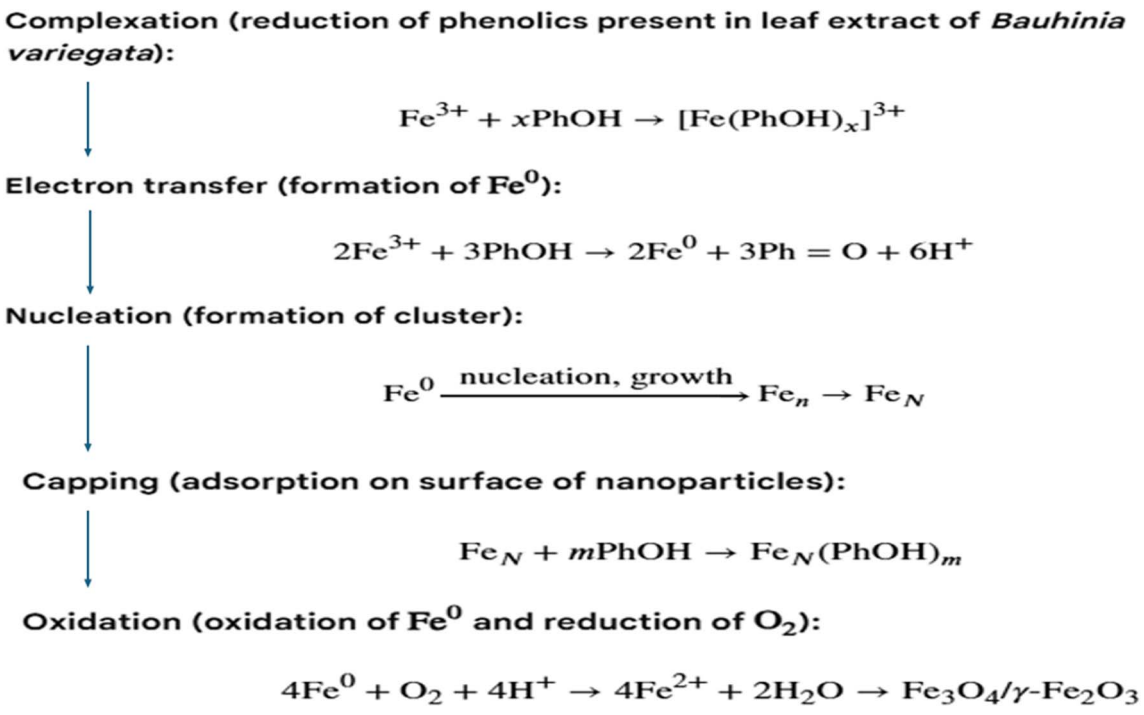


Fig. 1 Schematic of the mechanism of synthesis of FeO nanoparticles using leaf extract of *B. variegata*.

plates and then dried for 5 minutes. Round wells were punctured in agar and then 0.1 ml of each concentration of FeO nanoparticles (125–1000 μg $ml^{-1}$) was added in respective wells followed by overnight incubation at 37 °C. The diameter of clear zones on plates across wells was determined. DMSO (2.0%) was used as a negative control, whereas wells containing ciprofloxacin was used as a positive control.

**2.3.2 Determination of MIC and MBC.** MIC (minimum inhibitory concentration) of FeO nanoparticles was estimated using a microtitration plate assay.[34] Two-fold serially diluted FeO nanoparticles (0–1000 μg $ml^{-1}$) in the LB broth were added. Then, 100 μl of standardized bacterial cultures (adjusted to 0.5 McFarland) were added in a microtiter plate having 100 μl of FeO nanoparticles in LB and incubated overnight at 37 °C. After incubation, 50 μl of nitro blue tetrazolium chloride (NBT) dye (5 mg $ml^{-1}$ concentration used) was dispensed in wells and the viability of bacteria was checked. NBT dye turns colour from yellow to bluish when the viable cells are present in the sample. As a result, the minimum concentration of FeO nanoparticles that inhibited change in colour was labelled as the MIC point. After MIC determination, 10 μl aliquot of each well indicating growth inhibition was spread over LB agar plates and incubated overnight at 37 °C. The plates were observed for bacterial growth, and the least concentration which killed bacteria was considered as MBC.

### 2.4 Tolerance level

To check the extent of bactericidal activity, the tolerance level of each bacterial strain was measured against FeO nanoparticles by using this relationship.[38,39]

$$\text{Tolerance} = \text{MBC/MIC}$$

### 2.5 Time kill assay

The time kill assay was performed to investigate the effect of different concentrations (0.5 × MIC, 1 × MIC and 2 × MIC) of FeO nanoparticles on the growth of bacterial isolates. Briefly, standardized bacterial culture (adjusted to 0.5 McFarland) was inoculated into an LB broth and grown in the presence of different concentrations of FeO nanoparticles at 37 °C. A growth control (without nanoparticle treatment) was also included. At different time intervals (0, 1, 2, 4, 8, 16 and 24 hours), the bacterial cell density was monitored by measuring the absorbance of cell culture at 600 nm.[37]

### 2.6 Antibiofilm potential of FeO nanoparticles

**2.6.1 Congo red agar assay.** The qualitative detection of slime production by bacteria was done by the Congo red agar (CRA) method.[40] For the preparation of media, brain heart infusion agar was supplemented with sucrose (5%) and Congo red dye (0.8 g per litre). The bacterial cultures were seeded onto the CRA plates having subinhibitory concentrations of FeO nanoparticles and incubated overnight at 37 °C. The control plates were not supplemented with nanoparticles. Following incubation, the colonies were observed for black color with dry consistency (strong slime producer) and pink colonies with mucoid consistency (weak slime producer).

**2.6.2 Crystal violet method.** The quantitative estimation of biofilms was performed by a crystal violet microtiter plate assay. Briefly, 24 hours old cultures were used after adjusting their turbidity to 0.5 McFarland. Then, 10 μl of different concentrations of FeO nanoparticles (0 × MIC, 0.5 × MIC and 1 × MIC) were added in 180 μl of the LB. A bacterial suspension (10 μl) was added into wells and incubated for 24 hours at 37 °C. Next, the contents of the wells were carefully decanted, washed thrice with normal saline and air-dried for 10 minutes. After that, the attached cells were fixed with methanol followed by staining with crystal violet (0.1%) for about 10 minutes. Again, the cells were washed with normal saline thrice to remove any unbound dye. Finally, the cells were suspended in 200 μl of 33% (v/v) glacial acetic acid to elute the dye. The biofilms were quantified by taking absorbance at 575 nm using an ELISA reader.[40]

The biofilm inhibition percentage was computed following this equation:

$$\text{Inhibition percentage} = [1 - \text{OD of treated cells (using nanoparticles)/OD of untreated cells}] \times 100$$

### 2.7 Antioxidant activity

The antioxidant activity of FeO nanoparticles was evaluated using different radical scavenging assays such as 2,2-diphenyl-1-picrylhydrazyl (DPPH), hydrogen peroxide ($H_2O_2$) and 2,2′-azino-bis(3-ethylbenzothiazoline-6-sulphonic acid) ABTS radical scavenging assay.

**2.7.1 DPPH method.** The antioxidant activity for FeO nanoparticles was checked following the previous protocol[41] by using different concentrations (12.5–100 μg $ml^{-1}$) of FeO nanoparticles and ascorbic acid (standard). Briefly, 200 μl of 0.1 mM DPPH reagent (in methanol) was mixed with 10 μl concentration of FeO nanoparticles. The suspension was incubated at 37 °C for 30 minutes in the dark followed by measuring the absorbance at 517 nm. The control (only methanol without nanoparticles) was also processed in a similar way. The percentage scavenging activity of nanoparticles was quantified using the following relationship:

$$\text{Antioxidant activity (\%)} = [(OD_C - OD_T)/(OD_C)] \times 100$$

where $OD_C$ denotes OD for control and $OD_T$ represents OD for treated/standard samples.

**2.7.2 ABTS method.** An ABTS solution (7 mM) was added to potassium persulfate (2.45 mM) in the same ratio and kept in dark for about 12 to 16 hours to prepare $ABTS^+$. The dilution of the ABTS working solution was done using methanol followed by mixing 4 ml of this dilution to FeO nanoparticles (10 μl). The mixture was kept in dark for about 30 minutes, and then the absorbance was measured at 734 nm. Ascorbic acid was used as the standard and processed in a similar way.[42]

**2.7.3 $H_2O_2$ method.** $H_2O_2$ assay was performed according to a protocol reported previously.[43] In a phosphate buffer saline, 20 mM solution of $H_2O_2$ was prepared (pH 7.4). Ascorbic acid and nanoparticles (1 ml) were separately mixed in 2 ml solution of $H_2O_2$ solution of PBS. The absorbance was measured at 230 nm after 10 minutes.

### 2.8 Photocatalytic activity

The photocatalytic action of FeO nanoparticles was evaluated by examining their ability to degrade Congo red dye.[44] The working solution (100 μg ml$^{-1}$) of dye was prepared from a stock solution having a concentration of 1 mg ml$^{-1}$. To estimate the photocatalytic activity, two parameters were considered, *i.e.*, first, the incubation time was varied while keeping the same concentration of FeO nanoparticles, and second, the concentration of FeO nanoparticles was changed while time was kept constant. In the first case, the same concentration of FeO nanoparticles (50 μg ml$^{-1}$) was used and added to working solutions by exposing to light for different time intervals, *i.e.*, 2 hours–10 hours. While in the second case, working solutions were combined with several concentrations of FeO nanoparticles (10 μg ml$^{-1}$–50 μg ml$^{-1}$) followed by incubation at room temperature for 10 hours. The dye decolourization was calculated by measuring the absorbance at 497 nm.

The dye degradation ability was investigated using the following equation:

$$\text{Decolorization (\%)} = [(\text{OD}_{\text{Control}} - \text{OD}_{\text{Sample}})/(\text{OD}_{\text{Control}})] \times 100$$

The kinetics plot was designed using (In $C_t/C_o$ *vs.* Time) to check the pseudo-first-order kinetics of Congo red dye degradation. $C_t$ is the concentration of the sample at that time and $C_o$ is the initial concentration of the sample.[45]

### 2.9 Statistical analysis

All experiments were conducted in triplicates and their findings were expressed as mean ± standard error. For data analysis, one-way analysis of variance (ANOVA) was used. Following the ANOVA, the post-hoc Tukey test was conducted to further analyse the differences between the groups using GraphPad Prism. A value of $p < 0.05$ was considered as significant difference.

## 3. Results

### 3.1 FeO nanoparticle synthesis and characterization

FeO nanoparticles were fabricated *via* a green route using aqueous leaf extract of *Bauhinia variegata* and were further characterized. The UV-visible spectroscopy for FeO nanoparticles displayed an absorption peak at 295 nm (Fig. 2A). XRD analysis indicated the presence of diffraction peaks at 2$\theta$ values of Bragg's angle for 30.90°, 35.30°, 44.50°, 48.90°, 53.79° and 62.75° (Fig. 2B), confirming the crystalline nature of iron oxide nanoparticles. The FTIR spectrum of biofabricated FeO nanoparticles is shown in Fig. 2C, where different peaks at 784, 1042, 1278, 1418, 1580, 1726, 2924, and 3600 cm$^{-1}$ were observed to confirm the presence of bioactive functional groups involved in the synthesis of FeO nanoparticles. The peak at 784 cm$^{-1}$ suggests the formation of the Fe–O bond. The peak at 1042 cm$^{-1}$ corresponds to the stretching vibration of C–O–C of polyphenolic compounds that might be present in the plant extract. The peak at 1278 cm$^{-1}$ demonstrated the presence of the OH group of primary/secondary alcohol, whereas the peak at 1580 and 1726 revealed the presence of C=C stretching and C=O, respectively, which might act as plant-based capping and reducing agents. An intense peak at 2924 was assigned to C–H methylene stretching, whereas an absorption peak at 3600 cm$^{-1}$ corresponds to the O–H stretching vibration of the polyphenolic group that might be involved in the formation and stabilization of nanoparticles. SEM micrograph showed the spherical or roughly spherical morphology of FeO nanoparticles with an average diameter of <100 nm (Fig. 2D).

### 3.2 *In vitro* antibacterial activity of FeO nanoparticles

**3.2.1 Agar well diffusion method.** The agar well diffusion method performed to assess the antibacterial activity of FeO nanoparticles clearly demonstrated a dose-dependent activity (by increasing the concentration, more growth inhibition was there) of nanoparticles against the tested bacterial strains. The results revealed statistically significant differences in the zone of inhibition across different bacterial strains and nanoparticle concentrations ($p < 0.05$). As presented in Table 1, the diameter of inhibitory zones lies in 7–25 mm range. The zone of inhibition varied across different concentrations of FeO nanoparticles (1000 μg ml$^{-1}$, 500 μg ml$^{-1}$, 250 μg ml$^{-1}$, and 125 μg ml$^{-1}$). Notably, *E. coli* exhibited the highest sensitivity, particularly at 1000 μg ml$^{-1}$ (25 ± 1.54) and 500 μg ml$^{-1}$ (21 ± 1.87), indicating its strong susceptibility to the nanoparticles. In contrast, *E. faecium* and *S. aureus* showed lower inhibition zones across all concentrations, with *E. faecium* at 125 μg ml$^{-1}$, demonstrating the least inhibition (07 ± 0.57). The nanoparticles showed broad-spectrum activity, with *A. baumannii* and *P. aeruginosa* displaying similar inhibition patterns at higher concentrations, suggesting the potential of these nanoparticles against MDR bacterial strains.

**3.2.2 Determination of MIC and MBC.** Further MIC and MBC of FeO nanoparticles were measured by using an NBT-based broth microdilution assay. It was noted that both Gram-positive and Gram-negative bacteria were susceptible to FeO nanoparticles. The results revealed that the MIC value of FeO nanoparticles for *A. baumannii*, *S. aureus* and *E. faecium* was 125 μg ml$^{-1}$; whereas for *E. coli*,*K. pneumoniae*, and *P. aeruginosa*, the MIC was found to be 62.5 μg ml$^{-1}$ (Table 1). Moreover, the MBC value was measured as the lowest concentration of FeO nanoparticles that did not allow bacteria to grow, and it ranged from 125 to 500 μg ml$^{-1}$ for all tested bacteria. The lowest MBC value (125 μg ml$^{-1}$) was found against *E. coli* and *P. aeruginosa* followed by *K. pneumoniae* and *A. baumannii* (250 μg ml$^{-1}$). The results, supported by an ANOVA $p$-value of 0.003, indicate statistically significant differences in susceptibility among the bacterial isolates.

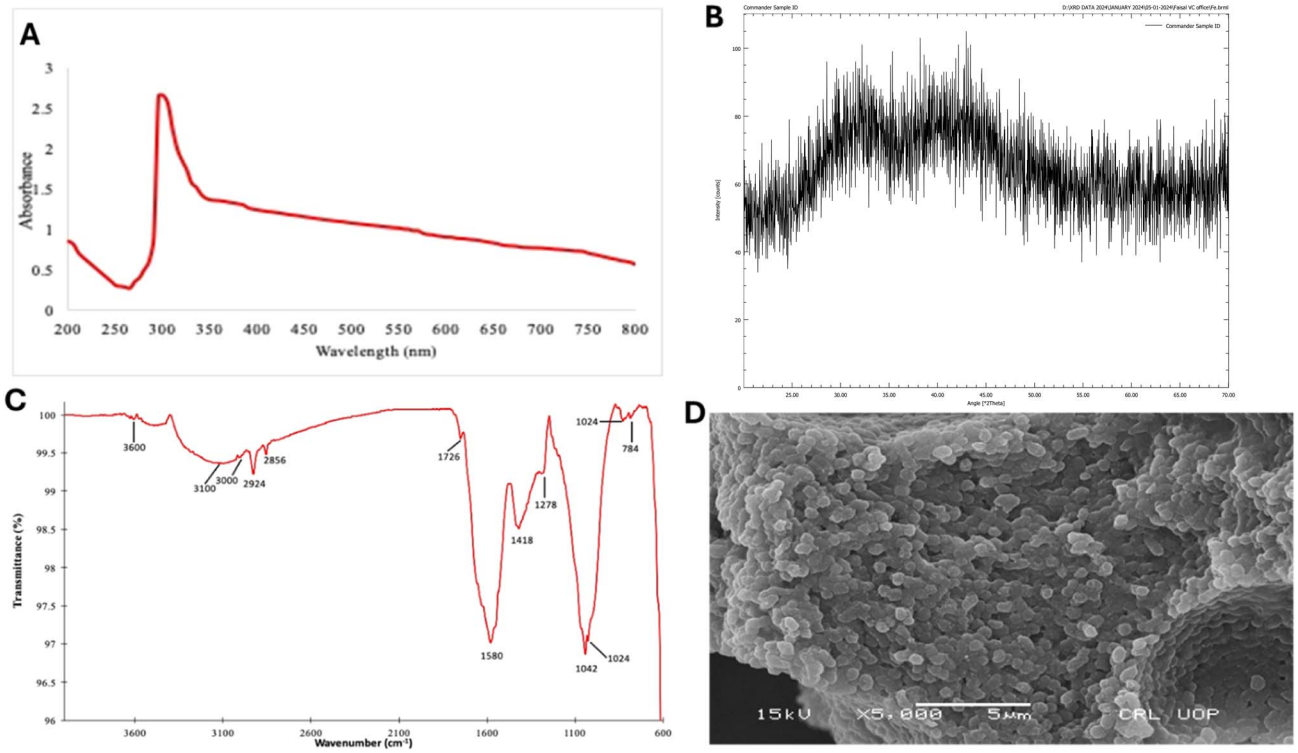


Fig. 2 Characterization of FeO nanoparticles by different techniques: (A) UV-visible spectrum of FeO nanoparticles, revealing absorbance (peak) at 295 nm. (B) XRD pattern of nanoparticles. (C) FTIR spectrum of biofabricated FeO nanoparticles revealing the presence of different functional groups. (D) SEM image of FeO nanoparticles.

**3.2.3 Tolerance level.** The tolerance level of each antibiotic-resistant bacteria was also measured for FeO nanoparticles. *E. coli* and *P. aeruginosa* were found to be the most susceptible, with both having an MIC of 62.5 μg ml$^{-1}$ and an MBC of 125 μg ml$^{-1}$, resulting in an MBC/MIC ratio of 2, indicating effective bactericidal action at lower concentrations. In contrast, *E. faecium* and *S. aureus* required higher concentrations, with MIC values of 125 μg ml$^{-1}$ and MBC values of 500 μg ml$^{-1}$, resulting in a higher MBC/MIC ratio of 4, suggesting that these strains are more resistant. The MBC/MIC ratio further supports that *K. pneumoniae*, *E. faecium*, and *S. aureus* may require higher nanoparticle concentrations for effective bactericidal action, indicating variability in nanoparticle efficacy across different bacterial species. These findings emphasize the potential of FeO nanoparticles in targeting antibiotic-resistant bacteria, although effectiveness varies depending on the bacterial strain (Table 1).

### 3.3 Time kill assay

The growth inhibitory effect of different concentrations of FeO nanoparticles (0×, 0.5×, 1×, 2 × MIC) against MDR bacterial isolates was checked at different time intervals, and the results are presented in Fig. 3a–f. It was noted that at a concentration of 0.5 × MIC, relatively high cell density was observed for cultures and as the concentration of NPs was increased, the growth curves revealed significant reduction in the pattern of growth in comparison to control cells (untreated). The highest reduction in the growth pattern was detected for *E. faecium* followed by *K. pneumoniae*, *S. aureus*, *E. coli*, *P. aeruginosa*, and *A. baumannii* at different concentrations, respectively (Fig. 3a–f).

Table 1 Zone of inhibition measured by well diffusion method and MIC and MBC values against MDR bacteria

| Bacterial isolates | Diameter of zone of inhibition (mm) at different conc. of FeO nanoparticles | | | | MIC of FeO nanoparticles (μg ml$^{-1}$) | MBC of FeO nanoparticles (μg ml$^{-1}$) | MBC/MIC |
|---|---|---|---|---|---|---|---|
| | 1000 μg ml$^{-1}$ | 500 μg ml$^{-1}$ | 250 μg ml$^{-1}$ | 125 μg ml$^{-1}$ | | | |
| *A. baumannii* | 24 ± 1.99 | 20 ± 1.69 | 15 ± 1.30 | 11 ± 0.91 | 125 ± 0.943 | 250 ± 0.003 | 2 ± 0.022 |
| *E. coli* | 25 ± 1.54 | 21 ± 1.87 | 15 ± 1.09 | 08 ± 0.60 | 62.5 ± 0.753 | 125 ± 0.933 | 2 ± 0.933 |
| *K. pneumoniae* | 23 ± 1.88 | 19 ± 1.52 | 14 ± 1.15 | 09 ± 0.43 | 62.5 ± 0.292 | 250 ± 0.892 | 4 ± 0.853 |
| *P. aeruginosa* | 24 ± 1.52 | 20 ± 1.91 | 15 ± 1.30 | 11 ± 0.91 | 62.5 ± 0.854 | 125 ± 0.042 | 2 ± 0.984 |
| *E. faecium* | 23 ± 1.22 | 18 ± 1.15 | 13 ± 1.52 | 07 ± 0.57 | 125 ± 0.744 | 500 ± 0.954 | 4 ± 0.843 |
| *S. aureus* | 22 ± 1.156 | 19 ± 1.2 | 12 ± 0.82 | 09 ± 0.96 | 125 ± 0.042 | 500 ± 0.833 | 4 ± 0.892 |

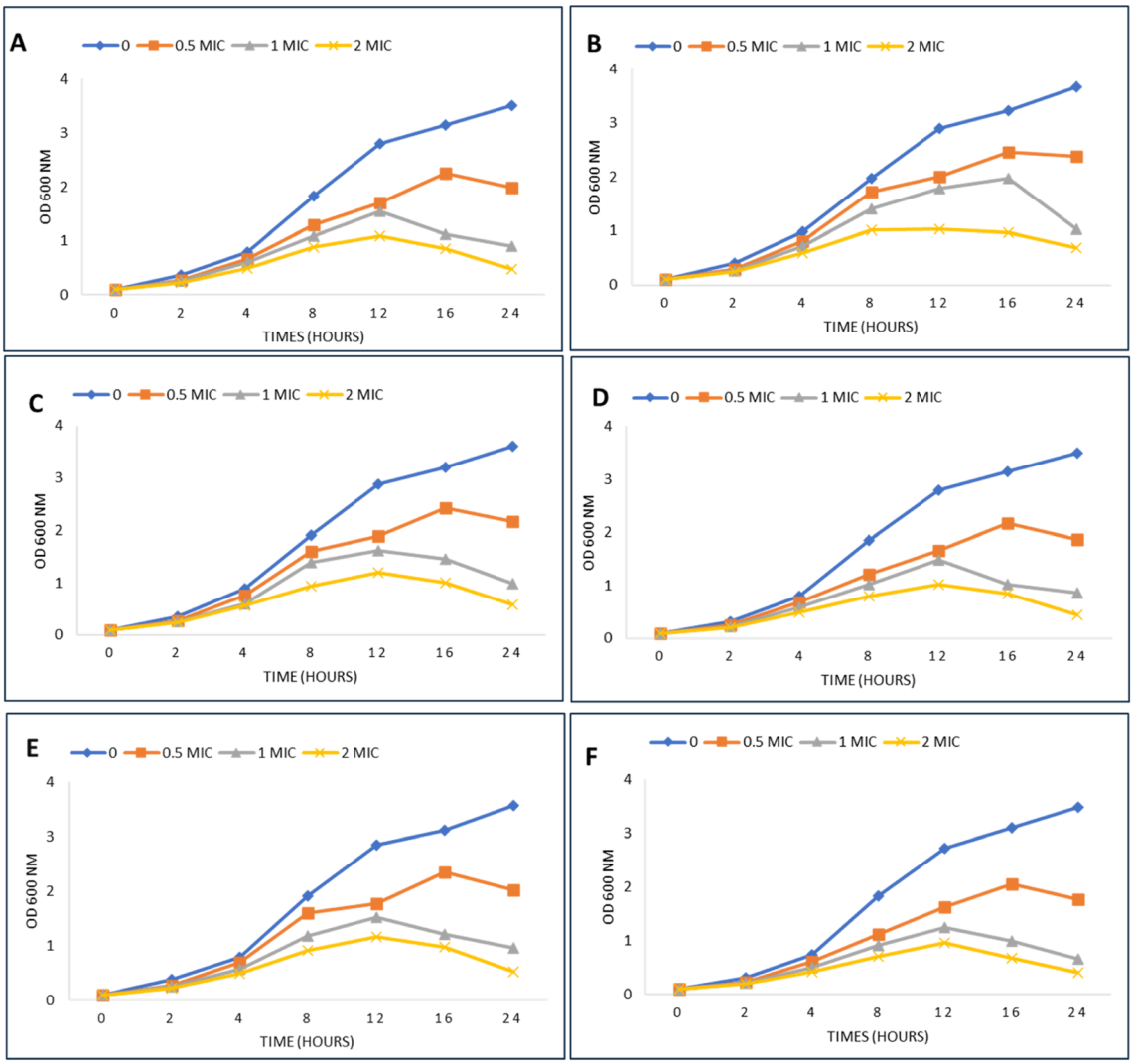


Fig. 3 Growth curve analysis representing the effect of different concentrations of FeO nanoparticles on MDR isolates: (A) *S. aureus*, (B) *A. baumannii*, (C) *E. coli*, (D) *K. pneumoniae*, (E) *P. aeruginosa*, and (F) *E. faecium*. Significant inhibition in bacterial growth was observed as the concentration of nanoparticles was increased.

### 3.4 Antibiofilm activity of FeO nanoparticles

**3.4.1 Congo red agar method.** Congo red agar assay was performed to see slime production of bacteria after exposing them to FeO nanoparticles at sub-inhibitory concentrations. It was observed that bacteria produced black colonies (indication of exopolysaccharide production) when grown in the absence of nanoparticles, as shown in Fig. 4a, whereas, when nanoparticles were added in an agar medium, slime production was hampered (as shown by pink colonies having mucoid appearance), although the growth of *K. pneumoniae* was not inhibited (Fig. 4b).

**3.4.2 Crystal violet method.** FeO nanoparticle antibiofilm activity was quantitatively evaluated by a crystal violet assay, and the results demonstrated a noteworthy inhibition of biofilm formation ($p < 0.05$) when cells were exposed to different concentrations of nanoparticles. The inhibitory effect is as follows: *E. coli* > *P. aeruginosa* > *A. baumannii* > *E. faecium* > *K. pneumoniae* > *S. aureus*. It was noted that inhibition (percentage) was in the range of 22.4–79.1% and the highest inhibition of 79.1% for *E. coli*, 75.87% for *P. aeruginosa*, 73.8% for *A. baumannii*, 71.78% for *E. faecium*, 70.7% for *K. pneumoniae* and 69.77% for *S. aureus* were achieved at 1 × MIC of FeO nanoparticles (Fig. 4C), and the OD value of FeO nanoparticles against MDR bacteria is shown in Fig. 4D.

### 3.5 Antioxidant activity

The antioxidant activity for FeO nanoparticles was measured by using DPPH, ABTS and $H_2O_2$ methods, and the results revealed that these nanoparticles presented significant differences in antioxidant activity ($p < 0.05$) across different tested concentrations and a notable improvement was seen at higher concentrations. The antioxidant value of ascorbic acid was in the range of 91.23–48.25%. The highest scavenging potential (89.09%) was observed in the case of DPPH method for FeO nanoparticles at 100 μg $ml^{-1}$ concentration in comparison to control. Moreover, for ABTS, the highest value achieved was

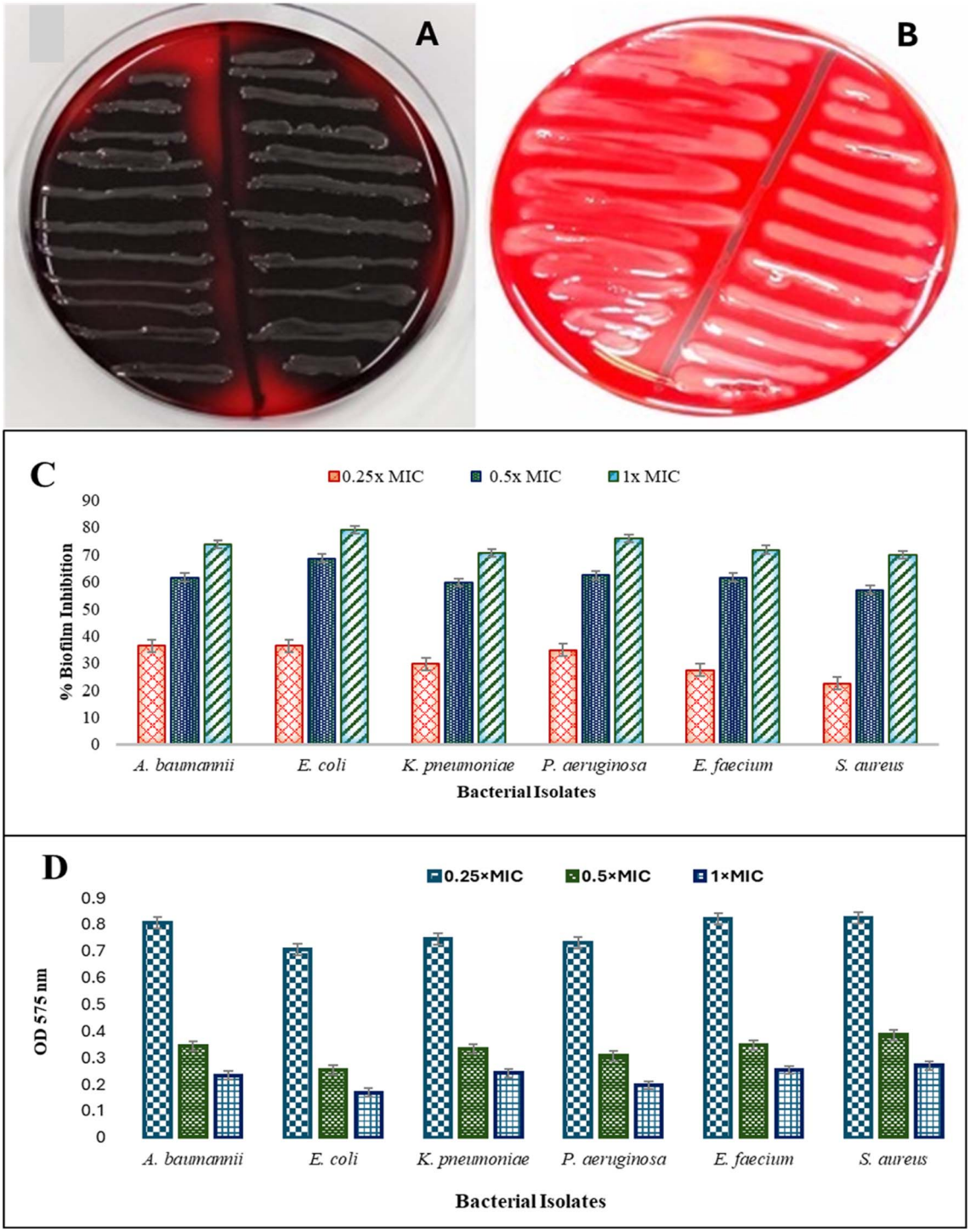


Fig. 4 Effect of FeO nanoparticles on slime production: (A) Control cells of *K. pneumoniae* having black colonies on a Congo red agar plate (indication of exopolysaccharide production). (B) Slime production was inhibited by FeO nanoparticles (as shown by pink colonies with mucoid appearance), though growth of bacteria was not inhibited. (C) Antibiofilm activity of FeO nanoparticles at different concentrations against MDR bacteria using a crystal violet assay. * symbol indicates significant differences ($p < 0.05$) in biofilm inhibition at different tested concentrations. (D) OD value of FeO nanoparticles against MDR bacteria using a crystal violet assay.

74.17% at the same tested concentration. In the $H_2O_2$ method, the radical scavenging activity was found in the range of 24–69.86%, while for DPPH and ABTS methods, the scavenging potential was in the range of 38–79.09% and 30.61–74.17%, respectively, as shown in Table 2.

### 3.6 Photocatalytic activity

The photocatalytic action of FeO nanoparticles was assessed by evaluating Congo red dye degradation based on the concentration and exposure time. The results presented significant photocatalytic activity ($p < 0.05$) of FeO nanoparticles that was

Table 2 Free radical scavenging activity of FeO nanoparticles

| | Free radical scavenging activity (%) | | | |
|---|---|---|---|---|
| FeO nanoparticles concentration (μg ml$^{-1}$) | Ascorbic acid | DPPH method | ABTS method | $H_2O_2$ method |
| 12.5 | 48.25 ± 1.06 | 38 ± 1.41 | 30.61 ± 2.32 | 24 ± 1.73 |
| 25 | 66.95 ± 0.77 | 53.05 ± 3.60 | 48.16 ± 2.01 | 36.72 ± 2.24 |
| 50 | 75.6 ± 2.36 | 70 ± 2.64 | 58.09 ± 1.93 | 51 ± 4.90 |
| 75 | 85.94 ± 2.18 | 81.01 ± 3.29 | 69.65 ± 1.46 | 68.1 ± 2.34 |
| 100 | 91.23 ± 2.738 | 89.09 ± 2.983 | 74.17 ± 1.29 | 78.86 ± 3.06 |

increased by increasing the nanoparticle concentrations and incubation time. As depicted in Fig. 6a, by increasing the incubation time (while keeping the dye concentration constant), the photocatalytic potential of nanoparticles was enhanced and the maximum dye degradation (72%) was achieved after 10 hours of incubation, while 53% dye degradation was observed after 8 hours. However, by keeping time constant (10 hours) and by changing the concentration of nanoparticles, 51% dye degradation was noted when nanoparticles were used in the concentration of 30 μg ml$^{-1}$, while the highest dye degradation (89%) was accomplished at a concentration of 50 μg ml$^{-1}$. The red line represents the concentration of dye left in the sample, whereas the blue line signifies the percent dye degradation. The graphs clearly indicated an improvement in dye degradation (72%) and a significant reduction ($p < 0.05$) in dye concentration present in the sample at different time intervals (Fig. 5a), whereas, in Fig. 5b, the red line represents the concentration of dye remaining and blue line indicates dye degradation. In this case, the highest dye degradation achieved was 89%, at 50 μg ml$^{-1}$ concentration of nanoparticles by keeping the time constant. The kinetics plot designed using (In $C_t/C_o$ *vs.* Time) showed a straight line; as the $R^2$ values > 0.90 confirmed the pseudo-first-order kinetics of Congo red dye degradation and presented a linear relationship in both time-dependent and concentration-dependent cases (Fig. 6).

## 4. Discussion

In the current era, the widespread emergence of antibiotic resistance has posed a serious threat to public health, leading to millions of deaths all around the globe. The situation is worsening by the capacity of these disease-causing agents to form biofilms that further increase their resistance towards antimicrobial agents. Novel strategies that can target biofilm forming MDR pathogens are required and metal and metal oxide nanoparticles, owing to the small sizes have significant biological applications and can be used as antibacterial and antibiofilm agents.[46]

In this study, FeO nanoparticles were synthesized by employing an ecofriendly approach using aqueous leaf extract of *B. variegata*. Green synthesis of nanoparticles is an ecofriendly approach and plant-based nanoparticles are proved to be more biocompatible and safe since a variety of signature bioactive compounds are present in different parts of the plants that can be used as reducing, stabilizing and capping agents during the nanoparticle synthesis *via* a green route.[47,48] It has been reported that the secondary metabolites present in plants such as alkaloids, phenolics, tannins, and flavonoids also exhibit antimicrobial activities. Flavonoids are substances known to be produced by plants because of microbial infection, and in addition, they have antioxidant potential which protects against oxidative stress. The hydroxyl group in these flavonoids facilitates scavenging of free radicals. The antibacterial property of these compounds is based on their ability to make complexes with extra-cellular proteins and they also form complexes with the outer cell wall of bacteria, resulting in the disruption of bacterial membranes and inhibition of biofilm formation. Many higher plants also have non-toxic glycosidic compounds when converted into phenolics *via* hydrolysis, which are toxic to these bacterial pathogens. Terpenoids have been known to display antibacterial property, leading to the loss of cell membrane integrity. Hence, the presence of these plant

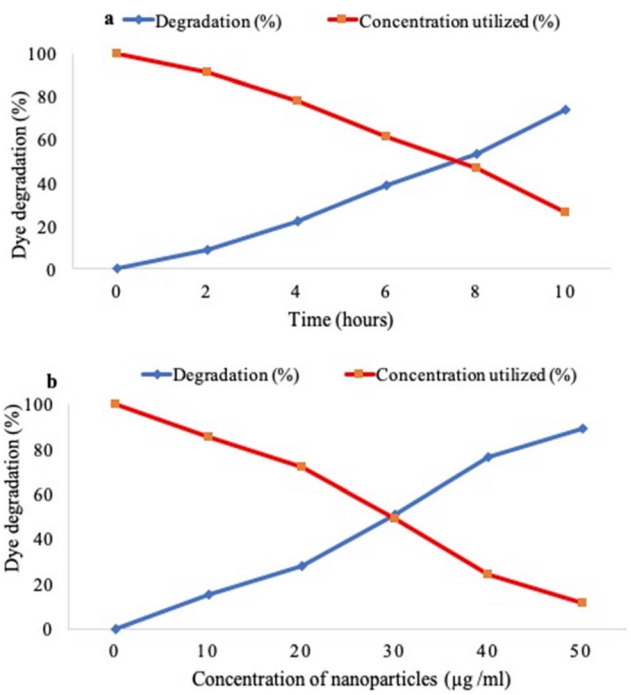


Fig. 5 Photocatalytic activity of FeO nanoparticles by examining their ability to degrade Congo red dye: (a) dye degradation at different time intervals by keeping the nanoparticle's concentration constant. (b) Dye degradation at different concentrations while keeping the time constant.

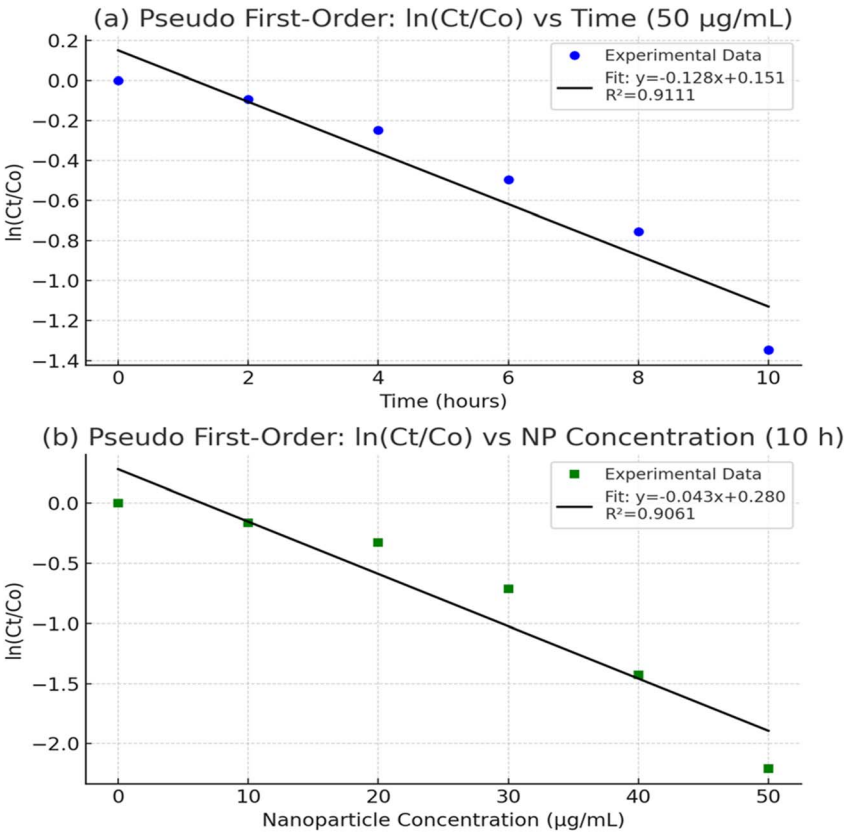


Fig. 6 Pseudo-first-order kinetics of FeO nanoparticles degrading Congo red dye: (a) Dye degradation at different time intervals by keeping the nanoparticle's concentration constant. (b) Dye degradation at different concentrations while keeping the time constant.

chemicals along with phenolics to some extent possibly justify the antibacterial, antibiofilm and antioxidant activities.[28,31]

The fabricated nanoparticles were characterized using different techniques, and the UV-visible spectroscopy revealed an absorption peak at 295 nm wavelength. Various studies have reported that the absorption peaks for FeO nanoparticles lie in the range of 250–300 nm; as Niraimathee *et al.*'s study showed a strong peak at 294 nm for iron oxide nanoparticles,[49] whereas Kiwumulo *et al.*'s study showed absorbance from 225 to 297 nm for FeO nanoparticles.[50] In another study, Rachida *et al.* also reported an absorption peak at 280 nm for iron oxide nanoparticles synthesized *via* a green route.[26] The XRD pattern confirmed the crystalline nature of the synthesized iron oxide nanoparticles and the observed peaks are consistent with the findings[51] who also demonstrated the crystalline nature of fabricated iron oxide nanoparticles. The FTIR spectra of nanoparticles showed significant peaks at 784, 1042, 1278, 1418, 1580, 1726, 2924, and 3600 $cm^{-1}$. The peak at 784 $cm^{-1}$ correspond to the Fe–O bond, as mentioned earlier.[51,52] The peak observed at 1042 $cm^{-1}$ corresponds to the stretching vibration of C–O–C of polyphenolic compounds that might be present in the *Bauhinia variegata* plant extract and are responsible for the reduction and ultimate synthesis of nanoparticles.[53] The absorption peak at 3600 $cm^{-1}$ correspond to the O–H stretching of the polyphenolic group that might be involved in the formation and stabilization of nanoparticles, whereas the peak at 1726 revealed the presence of carbonyl group C═O that might reflect the presence of secondary polyphenols.[54] In our study, the SEM image revealed the sphere-shaped biofabricated nanoparticles with an average diameter <100 nm. Yadav *et al.* (2020) also mentioned the sphere-shaped iron oxide nanoparticles with an average size of 38.9 nm.[55]

The biosynthesized FeO nanoparticles exhibited broad spectrum antibacterial activity against both Gram-positive and Gram-negative bacteria. Various studies have reported the antimicrobial potential of FeO nanoparticles.[56–58] The inhibition mechanism of bacteria is not fully understood; some of the studies suggested that FeO nanoparticles enter the cell to damage bacterial enzymes that leads to cell death.[59] It has been stated that biosynthesized FeO nanoparticles display efficient antimicrobial activity in comparison to chemically produced or commercially available nanoparticles, since, in general, most plants utilized for the synthesis of nanoparticles also have antibacterial properties.[60] Fe nanoparticles mostly induce oxidative stress by producing reactive oxygen species (ROS) directing the Fenton reaction that leads to intracellular oxygen or the production of hydrogen peroxide ($H_2O_2$) in the cell. Due to the generation of ROS, cell membrane disruption will occur and the cellular content might be leaked out. It has been stated that $H_2O_2$ might be produced from $Fe^{2+}$ in the presence of oxygen. Furthermore, Fe ions directly bind to DNA or cell proteins,

 

which might disturb cell replication and enzymatic activities and also result in the release of cellular components.[61]

When the nanoparticles interact with bacterial cells, they may encounter various biomolecules such as lipopolysaccharides (LPS), proteins, phospholipids and lipoteichoic acids present on the bacterial envelope. Consequently, the available functional groups on both bacterial envelopes and nanoparticle surface, combined with the physicochemical attributes of NPs, influence the possible toxic outcome for bacteria.[62] In the present study, FeO nanoparticles displayed significant antibacterial activity against both Gram-negative bacteria and Gram-positive bacteria; however, better inhibitory effects were observed against Gram-negative bacteria possibly due to the differences in their cell wall composition, as observed earlier as well.[63] FeO nanoparticles can bind to the formate hydrogenlyase (FHL) complex present in the cell walls of bacteria like *E. coli*. This interrupts the membrane's proton gradient, which is necessary for energy production and has a strong antimicrobial effect.[64–66] Gabrielyan *et al.* observed that iron oxide nanoparticles also showed antibacterial activity, which they linked to the unique structural features of bacterial cell walls.[67] In the time kill assay, the highest decline in bacterial growth was detected for *E. faecium* followed by *K. pneumoniae*, *S. aureus*, *E. coli*, *P. aeruginosa*, and *A. baumannii* at different concentrations, respectively. When the cells were grown in the presence of 1 × MIC and 2 × MIC concentrations of nanoparticles, a significant inhibition of bacterial growth was observed for all tested bacteria. The results were in accordance with other studies on *S. aureus*, *E. coli*, and *P. aeruginosa* where reduction in growth pattern was also noticed.[66,68,69]

The formation of biofilm provides higher resistance to bacteria, therefore underlying infection caused by these antibiotic-resistant bacteria is difficult to treat. Infection due to the biofilm formers usually stay longer and recur, leading to prolonged antibiotic therapy, or in some cases, the removal of these medical devices becomes mandatory. Bacterial adhesion to material surfaces, leading to the formation of biofilms, is facilitated by various non-specific interactions, including electrostatic forces, dipole–dipole interactions, hydrogen bonding, hydrophobic interactions, and van der Waals forces. Although various metal oxide nanoparticles can restrain the biofilms formed by resistant bacteria, and are hence, proved to be an effective means to treat clinical infections initiated through these bacteria. However, prior to evaluating any NP-mediated approach as a potential antibiotic, it is essential that the material exhibits antimicrobial properties to minimize microbial adhesion.[70–72]

In the current study, FeO nanoparticles efficiently reduced the formation of biofilm by MDR bacteria in a dose-dependent way and more than 70% inhibition was seen for selected bacteria. The mechanism for inhibitory effect has been seen owing to the poly-cationic nature of FeO.[73] In most of the bacteria, the biofilm has poly anionic nature;[74] thus, positively charged metallic nanoparticles counteract with the biofilm having negative charges *via* static actions to access the biofilm, whereas interrupt quorum sensing capacity and further restrain the development of biofilms.[75,76]

Some bacterial strains have the ability to produce slime, which promotes adhesion and biofilm formation on various surfaces. The Congo red agar assay was used to assess the slime production capacity of bacteria after exposing them to FeO nanoparticles (at sub-inhibitory concentrations). Our results revealed that bacteria produced black colonies (indication of exopolysaccharide production) when grown in the absence of nanoparticles; however, when nanoparticles were added in the agar medium, slime production was hampered. Selem *et al.* (2022) also demonstrated the inhibition of slime production in *E. coli*, when cells were exposed to silver nanoparticles that ultimately decreased the biofilm forming capacity of target bacteria.[77] In the current study, bacterial attachment to the surface was affected, which ultimately inhibited biofilm formation. As reported in the literature, FeO nanoparticles inhibit mature biofilms and prevent initial bacterial adhesion through multiple mechanisms, including damage from ROS, physical damage to cell membranes, and disruption of matrix. The combination of these effects provides a powerful strategy for combating biofilm production.[78]

Due to the role of free radicals in numerous pathologies, there has been a significant interest in the pursuit of novel antioxidants that can overcome the shortcomings of the endogenous defence system. In the current investigation, FeO nanoparticles were explored for their antioxidant potential by using different concentrations. The results revealed encouraging antioxidant capacity of nanoparticles, and these findings are in agreement with the study conducted by Sandhya & Kalaiselvam, (2020) who reported 43.04–85.53% radical scavenging potential of iron oxide nanoparticles, as measured by the DPPH assay.[79] The plausible explanation for enhanced activity was the presence of numerous secondary metabolites such as phenolics, glycosides, tannins and flavonoids in the plant extract, which lead to improved activity.[80] In addition, polyphenols present in the plant extract are responsible for their antioxidant potential due to the presence of OH groups in their chemical structure. These groups can readily donate electrons to cancel out damaging free radicals such as ROS. When polyphenols adsorb onto the surface of FeO nanoparticles, they set up a bioactive layer that precisely scavenge destructive radicals, substantially enhancing the antioxidant potential.[81]

Due to increasing anthropogenic activities, numerous pollutants originating from municipal, agricultural and industrial sources are infiltrating the natural ecological systems and food production. The photocatalytic activity of FeO nanoparticles can play a central role in ecological remediation such as the breakdown of industrial effluents, airborne pollutants, and toxic metabolites and in the treatment of wastewater. The photocatalytic action of FeO nanoparticles was evaluated with Congo red dye (an organic lethal pollutant present in the industrial waste) by adjusting the time of incubation and using various doses of FeO nanoparticles. It was observed that the maximum degradation of dye (72%) was achieved after 10 hours of incubation by keeping the dye concentration constant, while 89% degradation was seen at 50 μg $ml^{-1}$ concentration of Congo red dye at a fixed incubation time. These results are in accordance with the study results reported by Souhaila *et al.* (2022), where green-synthesized FeO nanoparticles catalyzed the azo dye degradation up to 98% within 60 minutes under the given experimental conditions.[82] It has been observed

that metal oxide nanoparticles, when used as photocatalysts, bind with dyes to reduce them.[21] The rate constant of the pseudo-first-order kinetics for Congo red dye appeared to be in agreement with the literature findings.[45] The mechanism works by exciting electrons from the valence band to the conduction band when the nanoparticles are exposed to light. This charge separation creates photocatalytically active sites on the surface of the nanoparticles. Further, the positively charged valence band reacts directly with water molecules to produce hydroxyl ions ($OH^-$). Meanwhile, the negatively charged electrons in the conduction band interact with dissolved oxygen to form superoxide anions. These reactive species then attach to the dye molecules, ultimately leading to their degradation.[83] It is found that the crystallinity, size and charge of nanoparticles substantially influence photocatalytic competence by changing the surface area and the availability of active sites. In general, the smaller the size, the greater the crystallinity, which improves the productivity by improving adsorption. This technique is extensively generalized to the degradation of pollutants and dyes present in wastewater.[84]

## 5. Conclusion

The current study explored the multifaceted applications of FeO nanoparticles, especially as antibiofilm, antioxidant and photocatalytic agents. The biomolecules within the *Bauhinia variegata* extract acted as reducing and capping agents, leading to the environmentally friendly, effective synthesis of FeO nanoparticles with distinct structural characteristics confirmed by various techniques. The promising *in vitro* outcomes position these green-synthesized FeO nanoparticles as a prospective competitor to counteract rising antimicrobial resistance and for environmental remediation. However, the study's *in vitro* nature necessitates immediate *in vivo* analyses to assess the biocompatibility, safety, and therapeutic efficacy in complex biological systems. Furthermore, there is a need to establish safe dosage levels and the evaluation of long-term side effects related to human and environmental exposure, including toxicity concerns. To perform industrial scaling, a well-controlled, safe and reproducible procedure is needed to guarantee the standardized quality of product throughout large batches.

## Author contributions

Rasti Abbas: conceptualization, investigation, and methodology. Saima Muzammil: data curation, writing-review and editing. Mohsin Khurshid: resources, writing-reviewing and editing. Sumreen Hayat: conceptualization, supervision, validation, writing-review and editing.

## Conflicts of interest

None to be declared.

## Data availability

The data used in this study can be provided from the corresponding author upon request.

## References

1 L. Serwecińska, Antimicrobials and Antibiotic-Resistant Bacteria: A Risk to the Environment and to Public Health, *Water*, 2020, **12**, 3313.
2 A. K. Singh, S. Das, S. Singh, V. R. Gajamer, N. Pradhan, Y. D. Lepcha and H. K. Tiwari, Prevalence of antibiotic resistance in commensal Escherichia coli among the children in rural hill communities of Northeast India, *PLoS One*, 2018, **13**, e0199179.
3 D. Swolana, M. Kępa, D. Idzik, A. Dziedzic, A. Kabała-Dzik, T. J. Wąsik and R. D. Wojtyczka, The Antibacterial Effect of Silver Nanoparticles on Staphylococcus Epidermidis Strains with Different Biofilm-Forming Ability, *Nanomaterials*, 2020, **10**, 1010.
4 D. I. Andersson, N. Q. Balaban, F. Baquero, P. Courvalin, P. Glaser, U. Gophna, R. Kishony, S. Molin and T. Tønjum, Antibiotic resistance: turning evolutionary principles into clinical reality, *FEMS Microbiol. Rev.*, 2020, **44**, 171–188.
5 N. Chakraborty, D. Jha, I. Roy, P. Kumar, S. S. Gaurav, K. Marimuthu, O.-T. Ng, R. Lakshminarayanan, N. K. Verma and H. K. Gautam, Nanobiotics against antimicrobial resistance: harnessing the power of nanoscale materials and technologies, *J. Nanobiotechnol.*, 2022, **20**, 375.
6 J. He, M. Hong, W. Xie, Z. Chen, D. Chen and S. Xie, Progress and prospects of nanomaterials against resistant bacteria, *J. Controlled Release*, 2022, **351**, 301–323.
7 H. F. Hetta, Y. N. Ramadan, A. I. Al-Harbi, E. A. Ahmed, B. Battah, N. H. Abd Ellah, S. Zanetti and M. G. Donadu, Nanotechnology as a Promising Approach to Combat Multidrug Resistant Bacteria: A Comprehensive Review and Future Perspectives, *Biomedicines*, 2023, **11**, 413.
8 I. E. Mba and E. I. Nweze, Nanoparticles as therapeutic options for treating multidrug-resistant bacteria: research progress, challenges, and prospects, *World J. Microbiol. Biotechnol.*, 2021, **37**, 108.
9 R. Abbasi, G. Shineh, M. Mobaraki, S. Doughty and L. Tayebi, Structural parameters of nanoparticles affecting their toxicity for biomedical applications: a review, *J. Nanopart. Res.*, 2023, **25**, 43.
10 Z. Alhalili, Metal Oxides Nanoparticles: General Structural Description, Chemical, Physical, and Biological Synthesis Methods, Role in Pesticides and Heavy Metal Removal through Wastewater Treatment, *Molecules*, 2023, **28**, 3086.
11 N. Hossain, M. H. Mobarak, A. Hossain, F. Khan, J. J. Mim and M. A. Chowdhury, Advances of plant and biomass extracted zirconium nanoparticles in dental implant application, *Heliyon*, 2023, **9**, e15973.
12 K. Q. Jabbar, A. A. Barzinjy and S. M. Hamad, Iron oxide nanoparticles: Preparation methods, functions, adsorption and coagulation/flocculation in wastewater treatment, *Environ. Nanotechnol., Monit. Manage.*, 2022, **17**, 100661.
13 N. Liaqat, N. Jahan, Khalil-ur-Rahman, T. Anwar and H. Qureshi, Green synthesized silver nanoparticles: Optimization, characterization, antimicrobial activity, and

cytotoxicity study by hemolysis assay, *Front. Chem.*, 2022, **10**, 952006.

14 R. B. Rotti, D. V. Sunitha, R. Manjunath, A. Roy, S. B. Mayegowda, A. P. Gnanaprakash, S. Alghamdi, M. Almehmadi, O. Abdulaziz, M. Allahyani, A. Aljuaid, A. A. Alsaiari, S. S. Ashgar, A. O. Babalghith, A. E. Abd El-Lateef and E. B. Khidir, Green synthesis of MgO nanoparticles and its antibacterial properties, *Front. Chem.*, 2023, **11**, DOI: **10.3389/fchem.2023.1143614**.

15 J. Shi, C. Peng, Y. Yang, J. Yang, H. Zhang, X. Yuan, Y. Chen and T. Hu, Phytotoxicity and accumulation of copper oxide nanoparticles to the Cu-tolerant plant Elsholtzia splendens, *Nanotoxicology*, 2014, **8**, 179–188.

16 U. S. Ezealigo, B. N. Ezealigo, S. O. Aisida and F. I. Ezema, Iron oxide nanoparticles in biological systems: Antibacterial and toxicology perspective, *J. Colloid Interface Sci. Open*, 2021, **4**, 100027.

17 P. C. Nagajyothi, M. Pandurangan, D. H. Kim, T. V. M. Sreekanth and J. Shim, Green Synthesis of Iron Oxide Nanoparticles and Their Catalytic and *In Vitro* Anticancer Activities, *J. Cluster Sci.*, 2017, **28**, 245–257.

18 A. Ahmed, M. Usman, B. Yu, Y. Shen and H. Cong, Sustainable fabrication of hematite (α-Fe2O3) nanoparticles using biomolecules of Punica granatum seed extract for unconventional solar-light-driven photocatalytic remediation of organic dyes, *J. Mol. Liq.*, 2021, **339**, 116729.

19 S. Meneceur, A. Bouafia, S. E. Laouini, H. A. Mohammed, H. Daoudi, G. G. Hasan and C. Salmi, High-efficiency photocatalytic degradation of antibiotics and molecular docking study to treat the omicron variant of COVID-19 infection using biosynthesized ZnO@Fe3O4 nanocomposites, *Phys. Scr.*, 2023, **98**, 115926.

20 W. Ahmad, V. Singh, S. Ahmed and M. Nur-e-Alam, A comprehensive study on antibacterial antioxidant and photocatalytic activity of achyranthes aspera mediated biosynthesized Fe2O3 nanoparticles, *Results Eng.*, 2022, **14**, 100450.

21 C. Xu, O. U. Akakuru, J. Zheng and A. Wu, Applications of Iron Oxide-Based Magnetic Nanoparticles in the Diagnosis and Treatment of Bacterial Infections, *Front. Bioeng. Biotechnol.*, 2019, **7**, 141.

22 E. Derakhshani, A. Naghizadeh and S. Mortazavi-Derazkola, Biosynthesis of MnFe2O4@TiO2 magnetic nanocomposite using oleaster tree bark for efficient photocatalytic degradation of humic acid in aqueous solutions, *Environ. Sci. Pollut. Res.*, 2023, **30**, 3862–3871.

23 M. Azzi, I. Medila, I. Toumi, S. E. Laouini, A. Bouafia, G. G. Hasan, H. A. Mohammed, S. Mokni, A. Alsalme and A. Barhoum, Plant extract-mediated synthesis of Ag/Ag2O nanoparticles using Olea europaea leaf extract: assessing antioxidant, antibacterial, and toxicological properties, *Biomass Convers. Biorefin.*, 2024, **14**, 31309–31322.

24 R. I. Barbhuiya, P. Singha, N. Asaithambi and S. K. Singh, Ultrasound-assisted rapid biological synthesis and characterization of silver nanoparticles using pomelo peel waste, *Food Chem.*, 2022, **385**, 132602.

25 A. Selmani, D. Kovačević and K. Bohinc, Nanoparticles: From synthesis to applications and beyond, *Adv. Colloid Interface Sci.*, 2022, **303**, 102640.

26 Z. A. Rachida, S. E. Laouini, C. Salmi, B. Abderrhmane, M. Souhaila, H. Mohammed, C. Soumaia, F. Alharthi and J. A. A. Abdullah, Green synthesis of α-Fe 2 O 3 and α-Fe 2 O 3 @Ag NC for degradation of rose Bengal and antimicrobial activity-Fe 2 O 3 @Ag NCs · α-Fe 2 O 3 NPs · Anti- candidiasis activity, *Biomass Convers. Biorefin.*, 2023, 3.

27 K. Sharma, V. Kumar, S. Kumar, R. Sharma and C. Mehta, Bauhinia variegata: a comprehensive review on bioactive compounds, health benefits and utilization, *Adv. Tradit. Med.*, 2021, **21**(4), 645–653.

28 M. Basumatari and B. N. Das, Karyomorphological studies in two species of Bauhinia Linn. and induction of polyploidy in Bauhinia acuminata Linn, *Int. J. Life Sci. Sci. Res.*, 2017, **3**, 1223–1229.

29 K. Sudheerkumar, S. Seetaramswamy, K. A. Babu and P. K. Kumar, Phyto pharmacognostical and isolation of chemical constituents from bauhinia variegata leaf extract, *J. Pharmacogn. Phytochem.*, 2015, **4**, 189–191.

30 R. Gonzalez-Pastor, S. E. Carrera-Pacheco, J. Zúñiga-Miranda, C. Rodríguez-Pólit, A. Mayorga-Ramos, L. P. Guamán and C. Barba-Ostria, Current Landscape of Methods to Evaluate Antimicrobial Activity of Natural Extracts, *Molecules*, 2023, **28**, 1068.

31 A. Mishra, A. K. Sharma, S. Kumar, A. K. Saxena and A. K. Pandey, Bauhinia variegata leaf extracts exhibit considerable antibacterial, antioxidant, and anticancer activities, *BioMed Res. Int.*, 2013, **2013**, 915436.

32 H. Obidah Abert, H. Umaru Aduwamai and S. Shehu Adamu, Effect of Green Synthesized Iron Oxide Nanoparticles Using Spinach Extract on Triton X-100-Induced Atherosclerosis in Rats, *Biochem. Res. Int.*, 2022, **2022**, 9311227.

33 S. Lakshminarayanan, M. F. Shereen, K. L. Niraimathi, P. Brindha and A. Arumugam, One-pot green synthesis of iron oxide nanoparticles from Bauhinia tomentosa: Characterization and application towards synthesis of 1, 3 diolein, *Sci. Rep.*, 2021, **11**, 8643.

34 S. Hayat, A. Ashraf, M. Zubair, B. Aslam, M. H. Siddique, M. Khurshid, M. Saqalein, A. M. Khan, A. Almatroudi, Z. Naeem and S. Muzammil, Biofabrication of ZnO nanoparticles using Acacia arabica leaf extract and their antibiofilm and antioxidant potential against foodborne pathogens, *PLoS One*, 2022, **17**, e0259190.

35 S. Hayat, S. Muzammil, M. H. Rasool, Z. Nisar, S. Z. Hussain, A. N. Sabri and S. Jamil, In vitro antibiofilm and anti-adhesion effects of magnesium oxide nanoparticles against antibiotic resistant bacteria, *Microbiol. Immunol.*, 2018, **62**, 211–220.

36 J. A. A. Abdullah, L. Salah Eddine, B. Abderrhmane, M. Alonso-González, A. Guerrero and A. Romero, Green synthesis and characterization of iron oxide nanoparticles by pheonix dactylifera leaf extract and evaluation of their antioxidant activity, *Sustainable Chem. Pharm.*, 2020, **17**, 100280.

37 A. M. Shehabeldine, B. H. Amin, F. A. Hagras, A. A. Ramadan, M. R. Kamel, M. A. Ahmed, K. H. Atia and S. S. Salem, Potential Antimicrobial and Antibiofilm Properties of Copper Oxide Nanoparticles: Time-Kill Kinetic Essay and Ultrastructure of Pathogenic Bacterial Cells, *Appl. Biochem. Biotechnol.*, 2023, **195**, 467–485.

38 J. May, K. Shannon, A. King and G. French, Glycopeptide tolerance in Staphylococcus aureus, *J. Antimicrob. Chemother.*, 1998, **42**, 189–197.

39 J.-S. Lee, Y.-M. Bae, A. Han and S.-Y. Lee, Development of Congo red broth method for the detection of biofilm-forming or slime-producing *Staphylococcus* sp, *LWT–Food Sci. Technol.*, 2016, **73**, 707–714.

40 S. Wu, L. Huang, J. Head, D. Chen, I. Kong and Y. Tang, Phytotoxicity of Metal Oxide Nanoparticles is Related to Both Dissolved Metals Ions and Adsorption of Particles on Seed Surfaces, *J. Pet. Environ. Biotechnol.*, 2012, **3**(4), DOI: **10.4172/2157-7463.1000126**.

41 A. A. Bhutto, Ş. Kalay, S. T. H. Sherazi and M. Culha, Quantitative structure-activity relationship between antioxidant capacity of phenolic compounds and the plasmonic properties of silver nanoparticles, *Talanta*, 2018, **189**, 174–181.

42 M. M. Abomughaid, Exploring a Sustainable Approach to Antioxidant Potential of Iron Oxide Nanoparticles Synthesized Using Citrus sinensis Peel Extract, *JOM*, 2023, **75**, 5388–5393.

43 C. D. Fernando and P. Soysa, Optimized enzymatic colorimetric assay for determination of hydrogen peroxide (H2O2) scavenging activity of plant extracts, *MethodsX*, 2015, **2**, 283–291.

44 S. Chatterjee, N. Guha, S. Krishnan, A. K. Singh, P. Mathur and D. K. Rai, Selective and Recyclable Congo Red Dye Adsorption by Spherical Fe3O4 Nanoparticles Functionalized with 1,2,4,5-Benzenetetracarboxylic Acid, *Sci. Rep.*, 2020, **10**, 111.

45 R. Jain, S. Mendiratta, L. Kumar and A. Srivastava, Green synthesis of iron nanoparticles using Artocarpus heterophyllus peel extract and their application as a heterogeneous Fenton-like catalyst for the degradation of Fuchsin Basic dye, *Curr. Res. Green Sustainable Chem.*, 2021, **4**, 100086.

46 P. Das, S. Ghosh and B. Nayak, Phyto-fabricated Nanoparticles and Their Anti-biofilm Activity: Progress and Current Status, *Front. Nanotechnol.*, 2021, **3**, 739286.

47 S. Faisal, H. Jan, S. A. Shah, S. Shah, A. Khan, M. T. Akbar, M. Rizwan, F. Jan, null Wajidullah, N. Akhtar, A. Khattak and S. Syed, Green Synthesis of Zinc Oxide (ZnO) Nanoparticles Using Aqueous Fruit Extracts of Myristica fragrans: Their Characterizations and Biological and Environmental Applications, *ACS Omega*, 2021, **6**, 9709–9722.

48 M. Khoobchandani, K. K. Katti, A. R. Karikachery, V. C. Thipe, D. Srisrimal, D. K. Dhurvas Mohandoss, R. D. Darshakumar, C. M. Joshi and K. V. Katti, New Approaches in Breast Cancer Therapy Through Green Nanotechnology and Nano-Ayurvedic Medicine - Pre-Clinical and Pilot Human Clinical Investigations, *Int. J. Nanomed.*, 2020, **15**, 181–197.

49 V. A. Niraimathee, V. Subha, R. S. E. Ravindran and S. Renganathan, Green synthesis of iron oxide nanoparticles from Mimosa pudica root extract, *Int. J. Environ. Sci. Dev.*, 2016, **15**, 227.

50 H. F. Kiwumulo, H. Muwonge, C. Ibingira, M. Lubwama, J. B. Kirabira and R. T. Ssekitoleko, Green synthesis and characterization of iron-oxide nanoparticles using Moringa oleifera: a potential protocol for use in low and middle income countries, *BMC Res. Notes*, 2022, **15**, 149.

51 N. Lal, M. Seifan, A. Ebrahiminezhad and A. Berenjian, The Effect of Iron Oxide Nanoparticles on the Menaquinone-7 Isomer Composition and Synthesis of the Biologically Significant All-Trans Isomer, *Nanomaterials*, 2023, **13**, 1825.

52 J. A. Thomas, F. Schnell, Y. Kaveh-Baghbaderani, S. Berensmeier and S. P. Schwaminger, Immunomagnetic separation of microorganisms with iron oxide nanoparticles, *Chemosensors*, 2020, **8**, 17.

53 A. Mohamed, R. R. Atta, A. A. Kotp, F. I. Abo El-Ela, H. Abd El-Raheem, A. Farghali, D. H. M. Alkhalifah, W. N. Hozzein and R. Mahmoud, Green synthesis and characterization of iron oxide nanoparticles for the removal of heavy metals (Cd2+ and Ni2+) from aqueous solutions with Antimicrobial Investigation, *Sci. Rep.*, 2023, **13**, 7227.

54 Y. Li, D. Kong and H. Wu, Analysis and evaluation of essential oil components of cinnamon barks using GC–MS and FTIR spectroscopy, *Ind. Crops Prod.*, 2013, **41**, 269–278.

55 V. K. Yadav, D. Ali, S. H. Khan, G. Gnanamoorthy, N. Choudhary, K. K. Yadav, V. N. Thai, S. A. Hussain and S. Manhrdas, Synthesis and Characterization of Amorphous Iron Oxide Nanoparticles by the Sonochemical Method and Their Application for the Remediation of Heavy Metals from Wastewater, *Nanomaterials*, 2020, **10**, 1551.

56 R. K. Bachheti, A. Fikadu, A. Bachheti and A. Husen, Biogenic fabrication of nanomaterials from flower-based chemical compounds, characterization and their various applications: A review, *Saudi J. Biol. Sci.*, 2020, **27**, 2551.

57 B. Das, S. Moumita, S. Ghosh, M. I. Khan, D. Indira, R. Jayabalan, S. K. Tripathy, A. Mishra and P. Balasubramanian, Biosynthesis of magnesium oxide (MgO) nanoflakes by using leaf extract of Bauhinia purpurea and evaluation of its antibacterial property against Staphylococcus aureus, *Mater. Sci. Eng. C*, 2018, **91**, 436–444.

58 G. A. Naikoo, M. Mustaqeem, I. U. Hassan, T. Awan, F. Arshad, H. Salim and A. Qurashi, Bioinspired and green synthesis of nanoparticles from plant extracts with antiviral and antimicrobial properties: A critical review, *J. Saudi Chem. Soc.*, 2021, **25**, 101304.

59 F. Buarki, H. AbuHassan, F. Al Hannan and F. Z. Henari, Green Synthesis of Iron Oxide Nanoparticles Using *Hibiscus rosa sinensis* Flowers and Their Antibacterial Activity, *J. Nanotechnol.*, 2022, **2022**, e5474645.

60 S. Kaviya, J. Santhanalakshmi and B. Viswanathan, Green Synthesis of Silver Nanoparticles Using *Polyalthia longifolia*

Leaf Extract along with D-Sorbitol: Study of Antibacterial Activity, *J. Nanotechnol.*, 2011, **2011**, e152970.

61 S. Fallah, E. Yusefi-Tanha and J. R. Peralta-Videa, Interaction of nanoparticles and reactive oxygen species and their impact on macromolecules and plant production, *Plant Nano Biol.*, 2024, **10**, 100105.

62 P. Patra, S. R. Choudhury, S. Mandal, A. Basu, A. Goswami, R. Gogoi, C. Srivastava, R. Kumar and M. Gopal, *Effect Sulfur and ZnO Nanoparticles on Stress Physiology and Plant (Vigna Radiata) Nutrition*, Springer Proceedings in Physics, 2013, pp. 301–309.

63 F. M. Abdulsada, N. N. Hussein, G. M. Sulaiman, A. Al Ali and M. Alhujaily, Evaluation of the Antibacterial Properties of Iron Oxide, Polyethylene Glycol, and Gentamicin Conjugated Nanoparticles against Some Multidrug-Resistant Bacteria, *J. Funct. Biomater.*, 2022, **13**, 138.

64 M. T. T. Thi, D. Wibowo and B. H. A. Rehm, Pseudomonas aeruginosa Biofilms, *Int. J. Mol. Sci.*, 2020, **21**, 8671.

65 J. Borcherding, J. Baltrusaitis, H. Chen, L. Stebounova, C.-M. Wu, G. Rubasinghege, I. A. Mudunkotuwa, J. C. Caraballo, J. Zabner, V. H. Grassian and A. P. Comellas, Iron oxide nanoparticles induce Pseudomonas aeruginosa growth, induce biofilm formation, and inhibit antimicrobial peptide function, *Environ. Sci.:Nano*, 2014, **1**, 123–132.

66 S. V. Gudkov, D. E. Burmistrov, D. A. Serov, M. B. Rebezov, A. A. Semenova and A. B. Lisitsyn, Do Iron Oxide Nanoparticles Have Significant Antibacterial Properties?, *Antibiotics*, 2021, **10**, 884.

67 L. Gabrielyan, A. Hovhannisyan, V. Gevorgyan, M. Ananyan and A. Trchounian, Antibacterial effects of iron oxide (Fe3O4) nanoparticles: distinguishing concentration-dependent effects with different bacterial cells growth and membrane-associated mechanisms, *Appl. Microbiol. Biotechnol.*, 2019, **103**, 2773–2782.

68 A. Alrashidi, M. Jafar, N. Higgins, C. Mulligan, C. Varricchio, R. Moseley, V. Celiksoy, D. M. J. Houston and C. M. Heard, A Time-Kill Assay Study on the Synergistic Bactericidal Activity of Pomegranate Rind Extract and Zn (II) against Methicillin-Resistant Staphylococcus aureus (MRSA), Staphylococcus epidermidis, Escherichia coli, and Pseudomonas aeruginosa, *Biomolecules*, 2021, **11**, 1889.

69 D. Baecker, Ö. Sesli, L. Knabl, S. Huber, D. Orth-Höller and R. Gust, Investigating the antibacterial activity of salen/salophene metal complexes: Induction of ferroptosis as part of the mode of action, *Eur. J. Med. Chem.*, 2021, **209**, 112907.

70 M. Agarwala, B. Choudhury and R. N. S. Yadav, Comparative Study of Antibiofilm Activity of Copper Oxide and Iron Oxide Nanoparticles Against Multidrug Resistant Biofilm Forming Uropathogens, *Indian J. Microbiol.*, 2014, **54**, 365–368.

71 M. Arakha, S. Pal, D. Samantarrai, T. K. Panigrahi, B. C. Mallick, K. Pramanik, B. Mallick and S. Jha, Antimicrobial activity of iron oxide nanoparticle upon modulation of nanoparticle-bacteria interface, *Sci. Rep.*, 2015, **5**, 14813.

72 M. S. A. Khan, M. M. Altaf and I. Ahmad, Chemical Nature of Biofilm Matrix and its Significance, in *Biofilms in Plant and Soil Health*, 2017, pp. 151–177, DOI: **10.1002/9781119246329.ch9**.

73 U. Teknologi MARA, N. L. Mohammad Mohaidin, F. Aris, U. T. MARA, I. M. Amin, U. T. MARA, N. Mohamad Zain, U. Teknologi MARA, N. Mohamed Yunus, U. Teknologi MARA, N. I. Taib and U. T. MARA, Antibiofilm Property of Green Synthesized Iron oxide Nanoparticles from Neem Leaves, *J. Sustainability Sci. Manage.*, 2022, **17**, 279–290.

74 D. H. Limoli, C. J. Jones and D. J. Wozniak, Bacterial Extracellular Polysaccharides in Biofilm Formation and Function, *Microbiol. Spectrum*, 2015, **3**(3), DOI: **10.1128/microbiolspec.MB-0011-2014**.

75 S. Sharma, J. Mohler, S. D. Mahajan, S. A. Schwartz, L. Bruggemann and R. Aalinkeel, Microbial Biofilm: A Review on Formation, Infection, Antibiotic Resistance, Control Measures, and Innovative Treatment, *Microorganisms*, 2023, **11**, 1614.

76 L. Shkodenko, I. Kassirov and E. Koshel, Metal Oxide Nanoparticles Against Bacterial Biofilms: Perspectives and Limitations, *Microorganisms*, 2020, **8**, 1545.

77 E. Selem, A. F. Mekky, W. A. Hassanein, F. M. Reda and Y. A. Selim, Antibacterial and antibiofilm effects of silver nanoparticles against the uropathogen *Escherichia coli* U12, *Saudi J. Biol. Sci.*, 2022, **29**, 103457.

78 M. Thukkaram, S. Sitaram, S. kumar Kannaiyan and G. Subbiahdoss, Antibacterial Efficacy of Iron-Oxide Nanoparticles against Biofilms on Different Biomaterial Surfaces, *Int. J. Biomater.*, 2014, **2014**, 716080.

79 J. Sandhya and S. Kalaiselvam, Biogenic synthesis of magnetic iron oxide nanoparticles using inedible borassus flabellifer seed coat: characterization, antimicrobial, antioxidant activity and *in vitro* cytotoxicity analysis, *Mater. Res. Express*, 2020, **7**, 015045.

80 N. sastry Yarla, J. I. Padmaja, R. P. Rao, K. Kirani, K. DSVGK, S. T. Devi, T. Parvathi, H. Gangadhar, S. K. Kumar and G. Duddukuri, In vitro dose dependent study on anti human pathogenic bacterial and free radical scavenging activities of methanolic seed coat extract of Borassus flabellifer L, *Asian J. Pharm. Clin. Res.*, 2012, **2**, 83–86.

81 N. V. Zagoskina, M. Y. Zubova, T. L. Nechaeva, V. V. Kazantseva, E. A. Goncharuk, V. M. Katanskaya, E. N. Baranova and M. A. Aksenova, Polyphenols in Plants: Structure, Biosynthesis, Abiotic Stress Regulation, and Practical Applications, *Int. J. Mol. Sci.*, 2023, **24**, 13874.

82 S. Meneceur, H. Hadia, A. Bouafia, S. E. Laouini, M. L. Tedjani, B. Djamila and M. S. Mahboub, Photocatalytic activity of iron oxide nanoparticles synthesized by different plant extracts for the degradation of diazo dyes Evans blue and Congo red, *Biomass Convers. Biorefin.*, 2024, **14**, 5357–5372.

83 M. Said, W. T. Rizki, W. R. Asri, D. Desnelli, A. Rachmat and P. L. Hariani, SnO2–Fe3O4 nanocomposites for the photodegradation of the Congo red dye, *Heliyon*, 2022, **8**, e09204.

84 K. K. Kefeni and B. B. Mamba, Photocatalytic application of spinel ferrite nanoparticles and nanocomposites in wastewater treatment: Review, *Sustainable Mater. Technol.*, 2020, **23**, e00140.